Structure, Vol. 13, 1035–1045, July, 2005, ©2005 Elsevier Ltd All rights reserved. DOI 10.1016/j.str.2005.04.010

Structural Basis of FFAT Motif-Mediated ER Targeting

Stephen E. Kaiser,[1] Jason H. Brickner,[2] Amy R. Reilein,[1] Tim D. Fenn,[1] Peter Walter,[2] and Axel T. Brunger[3,*]
[1]Department of Molecular and Cellular Physiology
Stanford University
Stanford, California 94305
[2]Howard Hughes Medical Institute and
Department of Biochemistry and Biophysics
University of California, San Francisco
San Francisco, California 94143
[3]Howard Hughes Medical Institute
Department of Molecular and Cellular Physiology
Department of Neurology and Neurological Sciences
Stanford Synchrotron Radiation Laboratory
Stanford University
James H. Clark Center E300-C
318 Campus Drive
Stanford, California 94305

Summary

The FFAT motif is a targeting signal responsible for localizing a number of proteins to the cytosolic surface of the endoplasmic reticulum (ER) and to the nuclear membrane. FFAT motifs bind to members of the highly conserved VAP protein family, which are tethered to the cytoplasmic face of the ER by a C-terminal transmembrane domain. We have solved crystal structures of the rat VAP-A MSP homology domain alone and in complex with an FFAT motif. The co-crystal structure was used to design a VAP mutant that disrupts rat and yeast VAP-FFAT interactions in vitro. The FFAT binding-defective mutant also blocked function of the VAP homolog Scs2p in yeast. Finally, overexpression of the FFAT binding-defective VAP in COS7 cells dramatically altered ER morphology. Our data establish the structural basis of FFAT-mediated ER targeting and suggest that FFAT-targeted proteins play an important role in determining ER morphology.

Introduction

The endoplasmic reticulum (ER) is a multifunctional organelle. After translocation across the ER membrane, secreted proteins fold, undergo posttranslational modification, and assemble into multiprotein complexes in the ER lumen (Baumann and Walz, 2001). Additionally, the cytosolic surface of the ER membrane is a major site for lipid biosynthesis, and many peripheral membrane proteins are localized to the cytosolic surface of the ER membrane (Baumann and Walz, 2001). While the mechanism by which proteins are targeted for translocation into the ER lumen is well characterized, it is not well understood how proteins are targeted to the cytosolic surface of the ER. Recent work has identified a targeting signal (the FFAT motif) responsible for targeting cytosolic proteins to the surface of the ER (Loewen et al., 2003) and to the nuclear membrane (Brickner and Walter, 2004). The FFAT motif (FFAT stands for diphenylalanine [FF] in an acidic tract) has the consensus amino acid sequence EFFDAxE (Loewen et al., 2003). This motif was identified because it is conserved in a large family of oxysterol binding protein-related proteins (ORPs) (Figure 1A and Figure S1A; see the Supplemental Data available with this article online [Loewen et al., 2003]). ORPs are regulators of lipid metabolism that are targeted by their FFAT motifs to the cytosolic surface of the ER (Loewen et al., 2003). In both yeast and mammals, proteins containing exposed FFAT motifs are targeted to ER membranes by interactions with VAP proteins (VAP stands for VAMP-associated protein; VAMP stands for vesicle-associated membrane protein) (Loewen et al., 2003; Wyles et al., 2002).

VAP proteins are composed of three conserved domains. These include an N-terminal immunoglobulin-like β sheet, a central coiled-coil domain, and a C-terminal transmembrane domain (Figure 1A). The N-terminal domain shares 22% sequence identity with the well-characterized major sperm protein (MSP) (Figure 1A and Figure S1B) (Roberts and Stewart, 2000). However, it is unclear whether VAP proteins share a common function. In metazoans, in addition to its role in recruiting FFAT motif-targeted proteins to ER membranes (Amarilio et al., 2005; Brickner and Walter, 2004; Kagiwada et al., 1998; Loewen and Levine, 2005; Loewen et al., 2003; Skehel et al., 2000; Soussan et al., 1999; Wyles et al., 2002; Wyles and Ridgway, 2004), VAP has been proposed to function in vesicle trafficking (Foster et al., 2000; Skehel et al., 1995), and in the organization of microtubule networks (Amarilio et al., 2005; Pennetta et al., 2002). Scs2p, the yeast homolog of VAP, binds FFAT motifs, and yeast lacking Scs2p mislocalize FFAT-targeted proteins to the cytoplasm (Loewen et al., 2003). In addition to its role in recruiting ORPs to the ER, Scs2p has also been implicated in transcriptional regulation of the *INO1* gene that encodes an important phospholipid biosynthetic protein (Brickner and Walter, 2004; Kagiwada et al., 1998). Strains lacking *SCS2* are unable to activate the *INO1* gene and cannot grow in the absence of inositol. Opi1p, a transcriptional repressor of *INO1* that possesses an FFAT motif (Figure 1A), is regulated by Scs2p on the nuclear membrane (Brickner and Walter, 2004; Loewen et al., 2003).

Here, we present the crystal structure for a VAP-FFAT motif interaction. We find that the specific molecular interactions between FFAT and VAP are highly conserved from yeast to mammals. Based on our structure of the VAP-FFAT complex, we designed mutants of the yeast VAP homolog Scs2p that are defective for FFAT motif binding. These mutants were defective for activation of *INO1*, indicating that FFAT-mediated binding of Scs2p to Opi1p is essential for this activation event. Finally, overexpression of wild-type VAP or of VAP de-

*Correspondence: brunger@stanford.edu

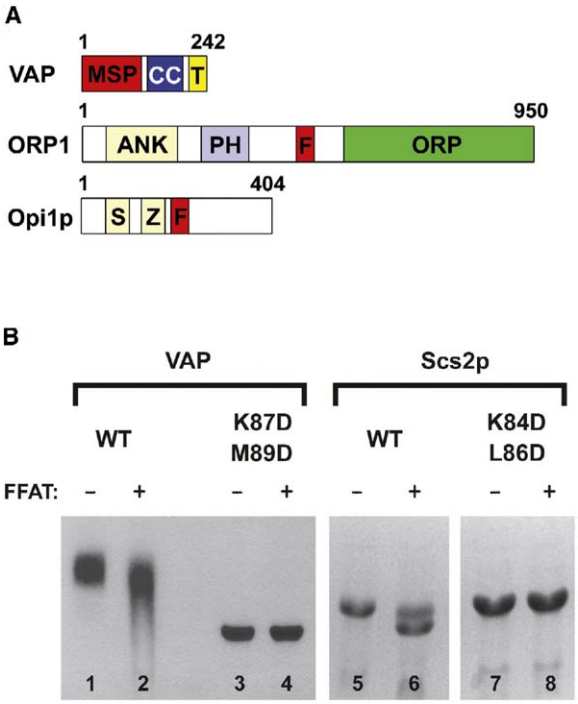

Figure 1. Domain Diagrams and Gel Shift Assays

(A) Domain organization diagrams of VAP, ORP1, and Opi1p. Domain abbreviations are: major sperm protein homology domain, MSP; coiled-coil domain, CC; transmembrane domain, T; ankyrin repeats, ANK; plekstrin homology domain, PH; FFAT motif with sequence related to EFFDAxE (Loewen et al., 2003), F; OSBP-related protein lipid binding domain, ORP; Sin3p binding domain, S; basic leucine zipper, Z.

(B) Native gel shift assay. VAP-A (1–125) alone (lane 1) migrates at a different rate than VAP-A (1–125) plus equimolar amounts of the ORP1 FFAT peptide SEDEFYDALS (lane 2), demonstrating that VAP-A (1–125) binds FFAT motifs directly. VAP-A (1–125) K87D/M89D migrates faster than VAP-A (1–125) (lanes 1 and 3). The mobility of VAP-A (1–125) K87D/M89D is not affected by added FFAT motif (lanes 3 and 4), suggesting that VAP K87D/M89D does not bind FFAT motifs. Yeast Scs2p binds to the FFAT motif peptide from yeast Opi1p (lanes 5 and 6). The yeast Opi1p peptide DDEEFFDASE caused a mobility shift of Scs2p (1–224) (lanes 5 and 6). The mobility of Scs2p (1–224) K84D/L86D is not affected by added peptide (lanes 7 and 8). FFAT peptides alone were not visible on the native gels used in these experiments.

fective for FFAT binding alters ER morphology in distinct patterns, suggesting that VAP and FFAT proteins play an important role in maintaining ER morphology.

Results and Discussion

VAP Interacts with Proteins Containing FFAT Motifs

To investigate VAP function, we analyzed the ability of VAP proteins to interact with putative binding partners that were suggested in previous reports (Pennetta et al., 2002; Skehel et al., 2000; Weir et al., 2001; Wyles et al., 2002). We were able to reproduce the reported interaction between VAP homologs and proteins containing FFAT motifs (Loewen and Levine, 2005; Loewen et al., 2003) with purified proteins in vitro. However, we found no evidence for direct interactions of cytosolic portions of VAP with cytosolic portions of SNARE proteins or with tubulin or microtubules (data not shown). The stoichiometry of the VAP-FFAT interaction was determined by size exclusion chromatography coupled to in-line multiangle laser light scattering (SEC-MALLS); recombinant rat ORP1 (454–546) (which contains the ORP1 FFAT motif) interacts with rat VAP-A (1–125) in a 1:1 complex (Figure S2). The interaction between VAP proteins and FFAT motifs was also confirmed by a native gel shift assay (Figure 1B). VAP-A (1–125) alone (lane 1) migrates at a different rate than VAP-A (1–125) plus equimolar amounts of the ORP1 FFAT peptide SEDEFYDALS (lane 2). We obtained similar results for the yeast Scs2p-Opi1p interaction (Figure 1B, lanes 5 and 6).

Crystal Structure of the Rat VAP-A MSP Homology Domain

In order to obtain a stable fragment of VAP-A that is suitable for crystallization, we performed limited trypsin digestion of the cytosolic portion of rat VAP-A (residues 1–219). We obtained a stable fragment consisting of VAP-A residues 1–123, as measured by MALDI mass spectrometry (data not shown). Secondary structure prediction (Rost and Liu, 2003) suggested that VAP-A residue 125 is the end of the β strand that contains residue 123. We thus expressed, purified, and crystallized VAP-A (1–125).

The crystal structure of selenomethionine-substituted rat VAP-A (1–125) was solved to d_{min} = 1.7 Å resolution using diffraction data from a multiwavelength anomalous dispersion (MAD) experiment (Table 1) (Hendrickson, 1991). As expected from sequence homology, the fold of VAP-A (1–125) is the same as that of MSP. Both are seven-stranded immunoglobulin-like β sandwiches with s-type topology, and their C_α backbones align with an rmsd of 2.0 Å over 109 residues (Bullock et al., 1996). Although they share the same fold and 22% sequence identity, VAP-A (1–125) and MSP have distinct surface electrostatic properties (Figure 2) and behave differently in solution. While MSP forms a symmetric dimer (Figures 2C and 2D) with a K_d of less than 50 nM (Haaf et al., 1996), VAP-A (1–125) is monomeric in solution, as measured by SEC-MALLS (Figure S2). VAP-A (1–125) crystallizes with one molecule in the asymmetric unit, but forms a symmetric crystal contact across a crystallographic 2-fold interface with a buried surface area of 440 Å^2. This interface is centered on a highly conserved sequence that contains Cys53. Cys53 residue pairs show a mixture of reduced and disulfide bonded conformations across this crystallographic interface. This disulfide bond may represent an artifact of crystallization. It is therefore noteworthy that VAP-A (1–125) is monomeric in solution and that, at the high protein concentration required for crystallization, none of the crystal contacts correspond to the MSP dimer interface. Indeed, critical residues in the MSP dimerization interface, such as Val18 and Tyr29, are not conserved in VAP proteins (Bullock et al., 1996). These residues are instead replaced in VAP-A by polar residues Lys17 and Thr28. We conclude that VAP MSP homology domains do not dimerize in the same way as MSP.

Table 1. VAP-A (1–125) Se-MAD Crystallographic Data Collection, Phasing, and Refinement Statistics

Crystallographic Data Statistics						
Space group				$P4_22_12$		
Cell dimensions				a = 48.2 Å, b = 48.2 Å, c = 112.4 Å		
	d_{min} (Å)	Number of Reflections	Completeness	<I>/<σ>	R_{sym}[a]	Multiplicity
λ1 inflection (0.9795 Å)	1.7	27,548	98.0 (99.8)[b]	16.5 (8.3)	10.1 (42.0)	12.9 (11.9)
λ2 peak (0.9793 Å)	1.7	27,537	98.1 (99.8)[b]	15.5 (7.8)	10.2 (41.0)	12.9 (12.1)
λ3 remote (0.9649 Å)	1.7	27,524	98.0 (99.8)[b]	17.2 (8.1)	9.8 (40.0)	12.9 (11.8)
MAD Phasing Statistics						
Observed Dispersive and Bijvoet Ratios[c]						
	λ1		λ2		λ3	
λ1	0.0585		0.0537		0.0749	
λ2			0.1146		0.0637	
λ3					0.0724	
Se-MAD Figure of Merit				0.79 (0.70)		
Refinement Statistics						
Resolution range				55–1.7 Å		
Number of reflections				27,484		
R[d]				22.1% (27.6%)		
R_{free}[e]				25.4% (30.0%)		
Luzatti coordinate error				0.22 Å		
Crossvalidated Luzatti coordinate error				0.26 Å		
Bond length deviation				0.005 Å		
Bond angle deviation				1.36°		
Average B factor				20.5 $Å^2$		
Bonded main chain atom B factor rmsd				1.45 $Å^2$		
Bonded side chain atom B factor rmsd				2.53 $Å^2$		
Residues in the most favored ϕ-ψ region				94.5%		
Residues in generously allowed region				5.5%		
Residues in disallowed region				0.0%		

[a] $R_{sym} = \Sigma_h\Sigma_i|I_i(h) - \langle I(h)\rangle|/\Sigma_h\Sigma_i|I_i(h)|$.
[b] Values in parentheses are for the highest resolution bin.
[c] Values are $\langle(\Delta|F|)^2\rangle^{1/2}/\langle|F|^2\rangle^{1/2}$, where $\Delta|F|$ is the dispersive (off-diagonal element), or Bijvoet difference (diagonal elements), computed between 500 and 1.7 Å resolution.
[d] $R = \Sigma(||F_{obs}| - k|F_{calc}||)/\Sigma|F_{obs}|$.
[e] R_{free} is the R value obtained for a test set of reflections, consisting of a randomly selected 10% subset of the diffraction data, not used during refinement.

Crystal Structure of a VAP-FFAT Complex

We next sought to determine the structural basis for the interaction between VAP proteins and FFAT motifs. We solved the structure of rat VAP-A (1–125) in complex with the rat ORP1 FFAT motif (residues 472-SEDEFYDALS-481) using diffraction data from a single wavelength anomalous dispersion (SAD) experiment and a native diffraction data set to d_{min} = 1.9 Å resolution (Table 2) (Hendrickson, 1991). The structure of VAP-A (1–125) is subtly changed by FFAT binding. VAP C_α backbones from our structures align with an rmsd of 1.3 Å over 113 residues. The FFAT motif binds across VAP β strands F, E, C, and D1 (Figure 3A). FFAT binding causes small (0.1–0.5 Å) changes in the position of backbone atoms within these β strands and substantial changes (2–4 Å) in the position of several side chain atoms that accommodate FFAT binding. We observed clear electron density for main and side chain atoms of ORP1 FFAT residues 476–481 and main chain atoms of residues 473–475 (Figure 3B). The FFAT residue Phe476 binds VAP in a hydrophobic pocket created by the aliphatic amino acid side chains of several residues (Figure 3B). It has extensive hydrophobic van der Waals contacts with VAP-A residue Met89 and with aliphatic portions of side chains from VAP-A residues Lys45, Thr47, Lys87, and Lys118 (Figure 3B).

The FFAT motif binds VAP on a positive patch that is in a highly conserved region on the VAP protein surface (Figures 3C and 3D). Part of the FFAT binding site on the yeast VAP homolog Scs2p was recently identified by a mutagenic screen (Loewen and Levine, 2005). This screen identified residues equivalent to VAP-A Lys45, Thr47, Lys87, and Lys118 as essential for VAP-FFAT interactions. Our structure reveals that, rather than interacting with negative side chains in FFAT motifs, aliphatic portions of these side chains form part of the hydrophobic pocket in which FFAT residue Phe476 binds. Additionally, our structure shows the full complement of VAP-FFAT interactions. FFAT residues 477 and 479–481 are bound to VAP by a network of backbone-backbone hydrogen bonds. Although the FFAT consensus sequence is EFFDAxE, the rat ORP1 FFAT sequence has the sequence 472-SEDEFYDALS-481. In our structure, FFAT residue Tyr479 is ordered but lacks substantial interactions with VAP. It is restrained by weak van der Waals interactions with several residues,

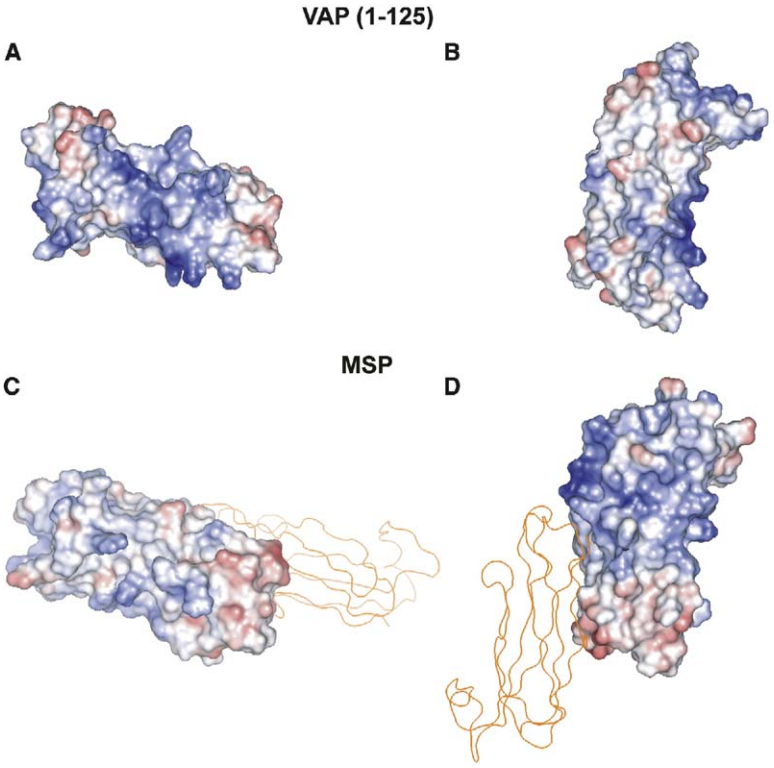

Figure 2. Comparison of Surface Electrostatic Characteristics of VAP-A (1–125) and MSP-1

(A and B) Two orientations of the VAP-A (1–125) monomer in surface representation colored to show the electrostatic potential calculated APBS, as implemented in Pymol by using the CHARMM force field. The electrostatic surface was contoured from –10 kT/e (red) to +10 kT/e (blue).

(C and D) Two orientations of the MSP-1 dimer equivalent to the VAP-A (1–125) orientations in (A) and (B) with one monomer in surface representation and the partner monomer in ribbon representation (orange). The MSP-1 surface is colored to show the electrostatic potential calculated by APBS, as implemented in Pymol using the CHARMM force field. The electrostatic surface was contoured from –10 kT/e (red) to +10 kT/e (blue).

and its γ hydroxyl group lacks a hydrogen bonding partner. This lack of strong interactions explains the observed variation between Phe or Tyr in the FFAT proteins identified to date and suggests that FFAT sequences with other residues at this position may be able to bind VAP. The side chain of Ala479 binds VAP in a small hydrophobic pocket created by aliphatic portions of side chains from residues Val44, Thr46, and Val54.

Although VAP-A (1–125) interacts with an FFAT motif as a 1:1 complex, as determined by SEC-MALLS (Figure S2), VAP-FFAT crystals are composed of two VAP MSP domains with two FFAT motifs bound between them (Figures 4A and 4B). As measured by SEC-MALLS, the VAP coiled-coil domain causes dimerization of VAP-A (1–219) (data not shown). The transmembrane domain, which contains the dimerization motif GxxxG (Russ and Engelman, 2000), is also likely to drive VAP dimerization. Thus, the observed crystal packing may mimic the high local VAP MSP homology domain concentration that would result from coiled-coil and transmembrane domain-induced VAP dimerization. Several additional observations corroborate this hypothesis. The VAP-VAP, VAP-FFAT, and FFAT-FFAT interactions within the 2:2 complex bury 1700 Å^2 of surface area and may explain the conservation of residues in FFAT motifs that are not explained by the 1:1 VAP-FFAT complex alone (Figure 4). In particular, of the residues in the EFFDAxE FFAT consensus sequence, the Asp following the single ring aromatic residues in FFAT motifs (Asp478 in ORP1) is strictly conserved among FFAT proteins identified to date (Figure S1A). Asp478 forms symmetric hydrogen bonds between the two FFAT motifs within a 2:2 complex (Figure 4C). These symmetric hydrogen bonds may explain the high conservation of Asp478 in FFAT motifs (Figure S1A). As described above, the side chain of FFAT residue Tyr477 is only weakly restrained by the VAP surface to which it is primarily bound. This residue is further restrained by a hydrophobic van der Waals contact with an aliphatic portion of the Asp478 side chain from the second FFAT motif within the 2:2 complex. Another argument for the relevance of the 2:2 complex is that it could form in the context of full-length VAP and full-length ORP1: the C termini of the two VAP-A (1–125) domains project from the same face of a 2:2 complex (Figure 4A), and the termini of the bound ORP1 peptide are oriented in a way that is consistent with VAP on membranes binding an FFAT motif of a large cytosolic protein (Figures 4A and 4B). Thus, the 2:2 complex could form between full-length VAP and FFAT proteins with both VAP coiled-coil domains dimerized and both VAP molecules tethered to the same membrane by their C-terminal transmembrane domains (Figure 4A).

FFAT Binding Is a Conserved VAP Function

The FFAT motif binding site is highly conserved among VAP protein family members but is not conserved in the structurally similar MSP-1 (Figure 3D). This observation prompted us to assess whether the yeast VAP homolog Scs2p interacts with FFAT motifs using the same molecular mechanism as that of rat VAP-A and to assess the functional significance of FFAT interactions for Scs2p function. We used the structure of the VAP-FFAT complex to construct point mutations on the surface of rat VAP-A that we predicted would specifically prevent FFAT binding. We chose to mutate two residues on the

Table 2. VAP-FFAT Complex: Crystallographic Data Collection, Phasing, and Refinement Statistics

Crystallographic Data Statistics						
Space group				P1		
Cell dimensions				a = 50.1 Å, b = 50.0 Å, c = 90.3 Å, α = 90°, β = 90°, γ = 60°		
	d_{min} (Å)	Number of Reflections	Completeness	<I>/<σ>	R_{sym}[a]	Multiplicity
Se-SAD (0.9794 Å)	2.8	37,329	99.0 (99.9)[b]	14.1 (9.4)	9.3 (21.0)	7.9 (7.8)
Native (1.0331 Å)	1.9	59,506	99.4 (100.0)[b]	10.2 (3.8)	6.0 (34.0)	4.0 (4.0)
SAD Phasing Statistics						
Se-SAD FOM				0.38 (0.34)		
Se-SAD FOMDM				0.84 (0.79)		
Refinement Statistics						
Resolution range				14.65–1.9 Å		
Number of reflections				53,477		
R[c]				21.5% (26.6%)		
R_{free}[d]				26.1% (32.3%)		
Luzatti coordinate error				0.20 Å		
Crossvalidated Luzatti coordinate error				0.18 Å		
Bond length deviation				0.031 Å		
Bond angle deviation				2.49°		
Average B factor				26.3 Å^2		
Bonded main chain atom B factor rmsd				1.79 Å^2		
Bonded side chain atom B factor rmsd				3.47 Å^2		
Average NCS rmsd (all atoms)				0.03 Å		
Residues in the most favored ϕ-ψ region				94.9%		
Residues in generously allowed region				5.1%		
Residues in disallowed region				0.0%		

[a] $R_{sym} = \Sigma_h \Sigma_i |I_i(h) - \langle I(h) \rangle| / \Sigma_h \Sigma_i |I_i(h)|$.
[b] Values in parentheses are for the highest resolution bin.
[c] $R = \Sigma(||F_{obs}| - k|F_{calc}||)/\Sigma|F_{obs}|$.
[d] R_{free} is the R value obtained for a test set of reflections, consisting of a randomly selected 10% subset of the diffraction data, not used during refinement.

VAP surface that interact with FFAT residue Phe476 (Figure 3B) to acidic residues by making the double point mutation K87D/M89D. As expected, in a native gel, the band corresponding to the VAP-A (1–125) K87D/M89D double mutant does not shift upon addition of the FFAT peptide (compare lanes 3 and 4 of Figure 1B). Wild-type and mutant VAP-A (1–125) are both folded, as measured by circular dichroism, and are both monodisperse and monomeric in solution, as measured by SEC-MALLS (data not shown).

Mutating the homologous residues (K84D/L86D) in the yeast VAP homolog Scs2p disrupted Scs2p interactions with the FFAT motif of the yeast protein Opi1p in vitro (Figure 1B, lanes 7 and 8). The gel shift experiments thus confirm that Scs2p residues K84 and L86 are equivalent to rat VAP-A residues K87 and M89 and that both proteins probably bind to FFAT motifs by the same mechanism. We next tested if the K84D/L86D mutant of Scs2p was functional in yeast. Strains lacking *SCS2* are unable to activate *INO1* and cannot grow in the absence of inositol. Expression of wild-type Scs2p in an *scs2Δ* mutant strain allowed activation of *INO1* and growth on medium lacking inositol. In contrast, Scs2p K84D/L86D failed to complement this growth phenotype (Figure 5A). Western blot analysis of total protein from yeast strains expressing wild-type or mutant Scs2p confirmed that the K84D/L86D mutant was expressed and stable in yeast (Figure 5B). Thus, the essential function of Scs2p in activating *INO1* requires its evolutionarily conserved FFAT binding activity.

Overexpression of VAP or an FFAT Binding Mutant Causes Altered ER Morphology

Several recent reports suggest that VAP-FFAT interactions may regulate ER morphology (Amarilio et al., 2005; Wyles et al., 2002; Wyles and Ridgway, 2004). VAP-A (1–242) overexpressed in COS7 cells as a C-terminal GFP fusion protein is localized to perinuclear and ER membranes and overlays with staining of the ER marker calreticulin (Figure 6A), but not with microtubules (Figure 6B). VAP-GFP overexpression resulted in the range of ER phenotypes illustrated in Figures 6A–6E. Overexpression of the VAP-A (1–242) K87D/M89D mutant, which disrupts FFAT binding, resulted in ER phenotypes ranging from those seen with overexpression of wild-type VAP to, in approximately 1%–10% of transfected cells, a pattern of regularly spaced patches of increased fluorescence as shown in Figures 6G and 6H. These patches are continuous with normal-appearing reticulated ER and colocalize with ER markers. This regular pattern of dense patches was never observed with overexpression of wild-type VAP. Since the K87D/M89D double point mutation does not affect VAP folding and structure or cause aggregation, it is likely that the observed pattern of dense patches results from the disruption of VAP-FFAT interactions.

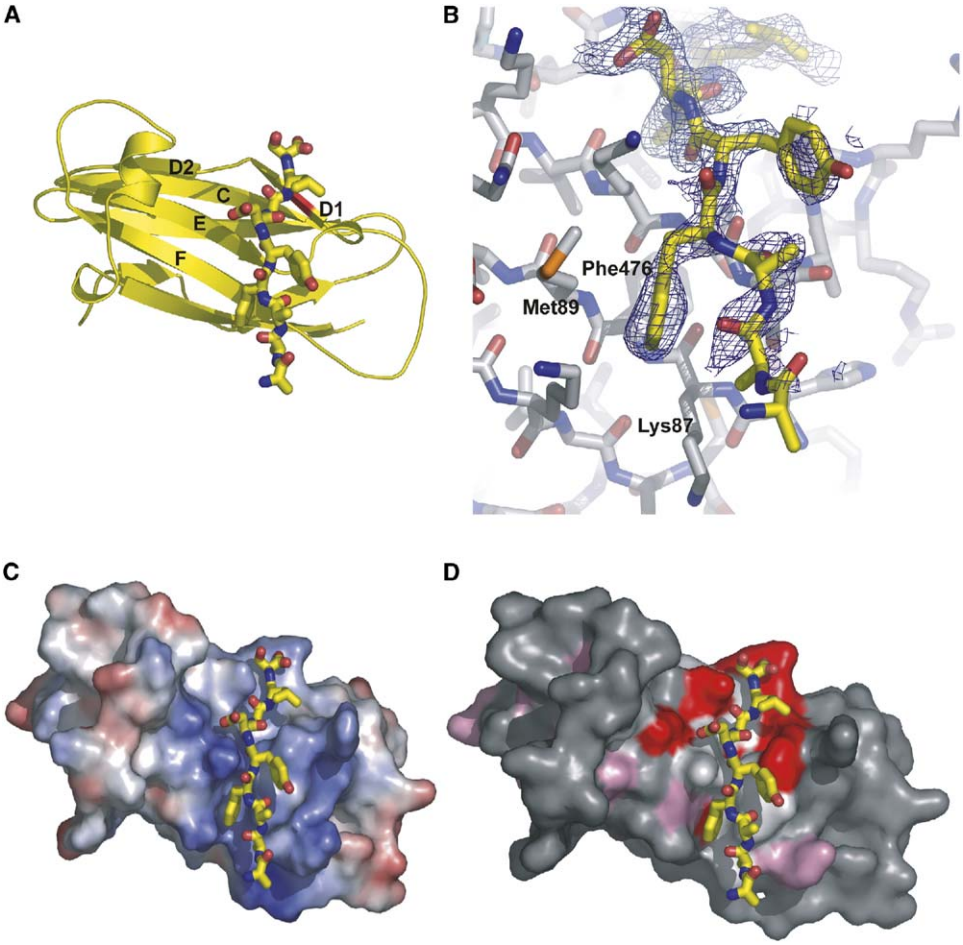

Figure 3. ORP1 FFAT Motif Interaction with the VAP-A (1–125) FFAT Binding Site

(A) The FFAT motif of ORP1 (shown in stick representation) binds across VAP-A (1–125) (shown in ribbon representation) β strands F, E, C, and D1.

(B) A zoomed view of VAP-A (1–125) (white carbon atoms) with bound FFAT motif (yellow carbon atoms) is shown in an orientation similar to that in (A). Electron density for the FFAT motif from a phase-combined, σ_A-weighted simulated annealing omit map that omitted FFAT peptide residues from map calculations is shown as blue mesh. ORP1 FFAT residue F476 binds in a cavity bordered by aliphatic side chains that include VAP Lys87 and Met89.

(C) The ORP1 FFAT motif binds VAP on a positive surface. The ORP1 FFAT peptide is shown in stick representation. VAP is oriented as in (A), and the surface is colored according to electrostatic potential as in Figure 2.

(D) The ORP1 FFAT motif binds in a region that is highly conserved among VAP homologs but not in the related protein MSP-1. Residues shown in red are identical among VAP homologs but are not conserved in MSP-1 and correspond to those marked with a red star in the alignment in Figure S1B. Residues shown in pink are similar among VAP homologs but are not conserved in MSP-1 and correspond to those marked with a pink triangle in the alignment in Figure S1B. Residues shown in white are conserved in VAP homologs and in MSP-1. Residues shown in gray are not conserved among VAP homologs.

Implications of the VAP-FFAT Interaction

The VAP-FFAT co-crystal structure reveals the structural basis for VAP binding of FFAT motif-containing proteins. We used the VAP-FFAT structure to design a stable VAP double point mutant that, although properly folded, is unable to bind FFAT motifs. We used this mutant to functionally characterize VAP-FFAT interactions and their conservation. We also characterized the effects of VAP protein overexpression on ER morphology in COS7 cells.

The VAP-FFAT structure should facilitate analysis of future questions concerning VAP interactions with FFAT motifs or with other proteins. For instance, we predict that a human isoform of VAP, VAP-C, is unable to bind FFAT motifs. Among other changes, VAP-C replaces Lys87 with His and Met89 with Ser. These changes are strikingly similar to those that we created in the K87D/M89D mutant that lacks FFAT binding.

It is conceivable that FFAT proteins compete for VAP interactions. Thus, the primary sequence variability and the relative affinities of various FFAT motifs (Figure S1A) that bind VAP proteins need to be analyzed. Our VAP-FFAT structure explains much, but not all, of the primary sequence conservation observed in FFAT motifs.

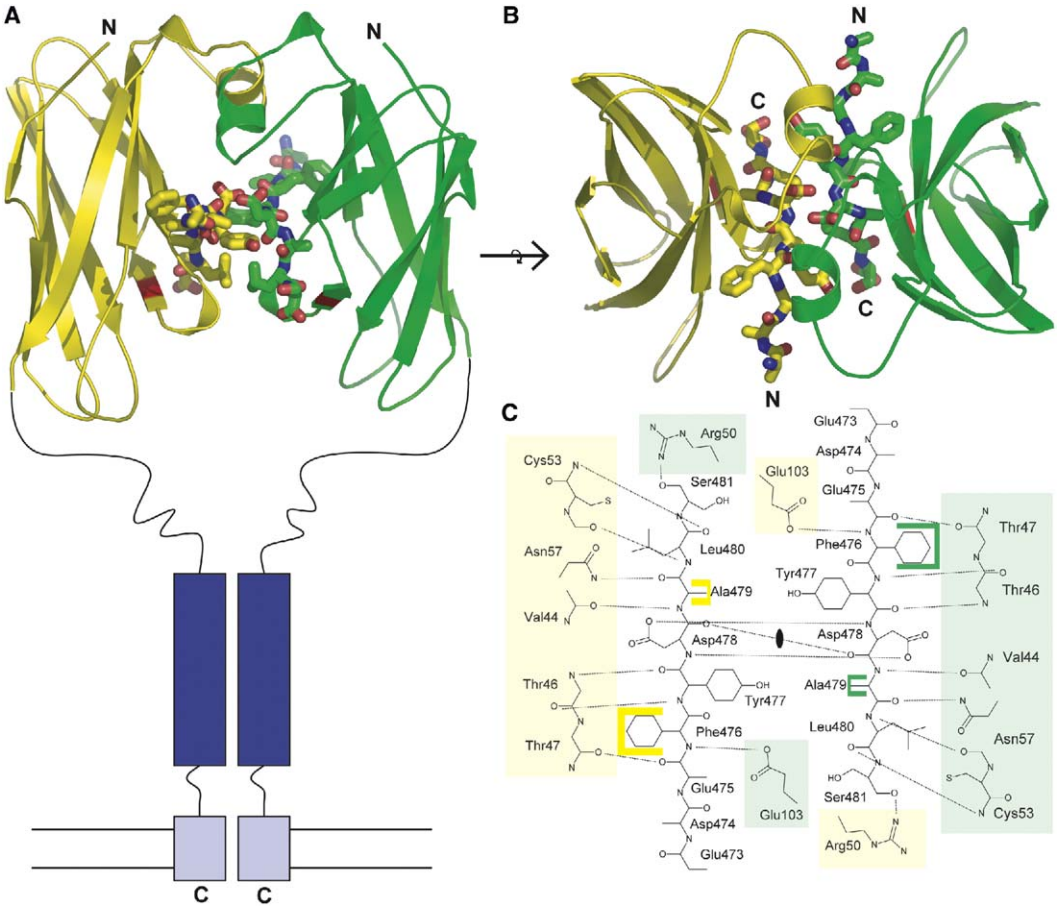

Figure 4. The VAP-FFAT 2:2 Complex

(A and B) The VAP-FFAT complex observed in the crystal structure buries two FFAT motifs (shown in stick representation) between two VAP-A (1–125) domains (shown in ribbon representation). (A) and (B) show the VAP-FFAT complex from two views related by the indicated 90° rotation. VAP residue Cys53 is colored red to orient the viewer. (A) illustrates a plausible orientation for the VAP-FFAT complex on membranes. VAP coiled-coil domains (residues 164–192) are shown in dark blue, and VAP transmembrane domains (residues 223–241) are shown in light blue.

(C) Schematic drawing of interactions between the two FFAT motifs and between VAP and FFAT motifs. This panel shows the same orientation as that in (B). The background behind VAP molecules is colored to match the VAP chains in (B). Hydrophobic van der Waals contacts are indicated by colored bars.

The primary VAP-FFAT interaction includes the first single ring aromatic residue in the EFFDAxE FFAT consensus sequence that binds in a hydrophobic cavity on VAP. The orientation of Phe476 in our structure suggests the possibility that FFAT motifs with Tyr at this position may still bind in a similar fashion. The secondary interactions in the 2:2 complex observed in VAP-FFAT crystals explain the high conservation of the Asp residue in the EFFDAxE FFAT consensus sequence. It is also noteworthy that the side chain for the first Glu in the EFFDAxE FFAT consensus sequence is not ordered in our structure. This may suggest that this residue is not absolutely conserved in FFAT motifs. Similarly, there are a variety of potential hydrogen bonding partners for the final Glu in the EFFDAxE FFAT consensus sequence. This coincides with the observed sequence heterogeneity within previously identified FFAT motifs. We propose that a less stringent definition of this motif sequence is required and that a wider variety of cytosolic proteins may be targeted to VAP on ER membranes than has been anticipated.

Experimental Procedures

Expression and Purification

DNAs encoding Rattus norvegicus VAP-A and ORP1 Δ41–130 were cloned using standard methodology from a brain cDNA library (Clontech) and were inserted into the pCR-Blunt II-TOPO vector (Invitrogen). Fragments corresponding to VAP amino acid residues 1–125 and 1–219 and ORP1 residues 454–546 were subcloned into the pGEX-4T expression vector (Pharmacia) and sequenced. Residues 1–125 or 1–219 of rat VAP or residues 454–546 of ORP1 were expressed as N-terminal glutathione-S-transferase (GST) fusion proteins in *E. coli*. BL21 (Novagen) cells were transformed with expression vector and were grown in a BIOFLO3000 fermenter (New Brunswick) to an OD_{600} of 30 in ECPYM1 media (Bernard and Payton, 1995) with 0.1 mg/ml ampicillin at 37°C. The temperature was shifted to 30°C, and heterologous protein expression was then initi-

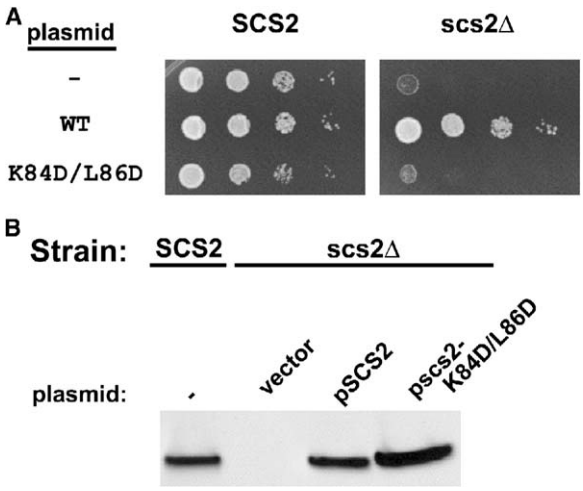

Figure 5. FFAT Binding Is a Major VAP Function that Is Conserved among Eukaryotes

Expression of a mutant of the yeast VAP homolog Scs2p that cannot bind the FFAT motif fails to complement the inositol auxotrophy of an *scs2*Δ yeast strain.

(A) Mutant *scs2*Δ strain was transformed with CEN/ARS plasmids expressing *SCS2* or *scs2*-K84D/L86D. The *scs2*Δ strain transformed with the empty vector failed to grow on media lacking inositol. Expression of wild-type Scs2p from the plasmid pSCS2 rescued this growth defect. Expression of the mutant Scs2p K84D/L86D failed to complement the growth phenotype, indicating that this mutant is unable to activate transcription of the *INO1* gene.

(B) Immunoblot analysis of Scs2p steady-state protein levels. Equal amounts of whole-cell yeast protein extract were separated by SDS-PAGE and transferred to nitrocellulose. Blots were probed with rabbit anti-Scs2p serum.

ated with 1 mM IPTG for 4 hr. Cells were harvested, flash frozen in liquid nitrogen, and stored at –80°C for later use. Selenomethionine-substituted protein was prepared by growing BL21 cells in M9 minimal media and inhibiting methionine biosynthesis in the presence of selenomethionine as described (Van Duyne et al., 1993). Expression was induced from the pGEX-4T vector by addition of 1 mM IPTG after the temperature was shifted from 37°C to 30°C at an OD_{600} of 1.5. After 4 hr of induction, cells were harvested, flash frozen, and stored for later use. For protein purification, 30 g frozen bacterial cells were resuspended in 200 ml lysis buffer consisting of 50 mM Tris (pH 8.0), 250 mM NaCl, 5 mM EDTA, and 10 mM DTT and were lysed using a pneumatic cell cracker at 16,000 PSI (Microfluidics). The lysate was then centrifuged in a JA-14 rotor (Beckman) at RCF (avg) 18,879 for 60 min, and the supernatant was incubated in batch with glutathione-sepharose resin (Pharmacia) at 4°C for 1 hr with gentle stirring. Fusion proteins were retained on the beads and were washed three times with four bed volumes of lysis buffer, then for three times with four bed volumes of thrombin buffer (50 mM Tris [pH 8.0], 250 mM NaCl, 13 mM 2-mercaptoethanol, 5 mM $CaCl_2$). The beads were then resuspended with thrombin buffer and incubated with ~50 μg bovine α-thrombin (Haematologic Technologies) at 4°C for 6 hr with slow mixing by rotation. After thrombin cleavage, the VAP or ORP1 protein-containing supernatants were dialyzed into mono-S buffer [50 mM MES buffer (pH 6), 50 mM NaCl, 10 mM DTT], respectively. VAP proteins were loaded onto a 10/10 mono-S column (Pharmacia) and eluted with a linear gradient of sodium chloride from 50 mM to 500 mM. ORP1 proteins were loaded onto a 10/10 mono-Q column (Pharmacia) and eluted with linear gradient of sodium chloride from 100 mM to 500 mM. VAP proteins were further purified by gel filtration chromatography on a Superdex 75 16/60 column (Pharmacia), then dialyzed into milli-Q water with 10 mM DTT and concentrated to 25 mg/mL before flash freezing small aliquots in liquid nitrogen for storage at –80°C. ORP1 proteins were dialyzed into 20 mM HEPES (pH 7.4), 100 mM NaCl, 10 mM DTT and concentrated to 25 mg/mL before flash freezing small aliquots in liquid nitrogen for storage at –80°C. Protein concentrations were calculated from absorbance measurements under denaturing conditions by using theoretical molar extinction coefficients.

Peptides corresponding to rat ORP1 residues 472–481 (SEDEFY DALS) and yeast Opi1p residues 197–206 (DDEEFFDASE) were synthesized by Biopeptide LLC. Peptides were resuspended in water before flash freezing small aliquots for later use.

Yeast Scs2p genomic DNA was amplified from genomic DNA and was inserted into the pCR-Blunt II-TOPO vector (Invitrogen). A fragment corresponding to Scs2p amino acid residues 1–224 was subcloned into the pet28c expression vector (Pharmacia) and sequenced. Scs2p (1–224) was expressed as an N-terminal 6xHis fusion protein in *E. coli*. BL21 (DE3) cells were transformed with expression vector and grown to an OD_{600} of 1.5 in LB medium with 0.1 mg/ml kanamycin at 37°C. The temperature was shifted to 30°C, and heterologous protein expression was then initiated with 1 mM IPTG for 5 hr. Cells were harvested, flash frozen in liquid nitrogen, and stored at –80°C for later use. For protein purification, cells were resuspended in lysis buffer consisting of 50 mM HEPES (pH 7.5), 150 mM NaCl, and 10 mM 2-mercaptoethanol and were lysed using a pneumatic cell cracker at 16,000 PSI (Microfluidics). The lysate was then centrifuged in a JA-14 rotor (Beckman) at RCF (avg) 18,879 for 60 min, and the supernatant was incubated in batch with Ni-NTA resin (Qiagen) at 4°C for 2 hr with gentle mixing. Fusion proteins were retained on the beads and were washed three times with four bed volumes of lysis buffer plus 20 mM imidazole, then for three times with four bed volumes of elution buffer (50 mM HEPES [pH 7.5], 150 mM NaCl, 10 mM 2-mercaptoethanol, 200 mM imidazole). Fractions containing fusion protein were then pooled and dialyzed into 50 mM HEPES (pH 7.5), 10 mM 2-mercaptoethanol overnight in the presence of ~50 μg bovine α-thrombin (Amersham Bioechnologies). Cleaved Scs2p protein was loaded onto a fast flow Hi-Trap Q (Pharmacia) column and eluted with a linear gradient of sodium chloride from 100 mM to 200 mM. Scs2p protein-containing fractions were pooled before flash freezing 25 μl aliquots in liquid nitrogen for storage at –80°C.

Protein Crystallization

Selenomethionine-substituted VAP-A (1–125) was thawed, and crystals were grown by vapor diffusion using sitting drops formed by mixing a 1:1 volume ratio of 25 mg/ml VAP with an equilibration buffer consisting of 30% polyethylene glycol monomethyl ether (molecular weight 2000), 200 mM NaCl, 25 mM Tris buffer (pH 7.5). Crystals formed over 1–3 weeks at 10°C in the space group $P4_22_12$, with unit cell dimensions a = b = 45 Å, c = 112 Å, and contained one molecule per asymmetric unit with 45% solvent. For crystallization of the VAP-FFAT motif complex, a 2:1 molar ratio of peptide:-VAP-A (1–125) was mixed to produce a protein solution with 2.5 mM peptide, 1.25 mM VAP, 6.8 mM DTT, 6.4 mM PIPES (pH 7.4). A small initial crystal grew in Hampton Research screen IndexHT condition H11, and subsequent crystals were grown by vapor diffusion using macroseeded sitting drops formed by mixing a 1:1 volume ratio of protein solution with an equilibration buffer consisting of 27% polyethylene glycol monomethyl ether (molecular weight 2000), 100 mM sodium thiocyanate, 100 mM Tris buffer (pH 7.4). Crystals formed in space group P1 (see below), with unit cell dimensions a = 50.1 Å, b = 50.0 Å, c = 90.3 Å, α = 90°, β = 90°, γ = 60°, and contained six molecules per asymmetric unit with 45% solvent.

Crystallographic Data Collection

Crystals were removed from sitting drops with a nylon loop and were transferred to a cryoprotectant solution composed of equilibration buffer supplemented with 15% ethylene glycol. Crystals were then flash frozen directly in a 100 K cryostream, and diffraction data were collected at beamline 8.2.1 of the Advanced Light Source using an ADSC Quantum-210 CCD detector. For the VAP-A (1–125) MAD experiment, oscillation diffraction data were collected to d_{min} = 1.7 Å resolution using inverse beam geometry in 15° wedges with all three wavelengths collected within each wedge (Table 1). For the VAP-FFAT complex, SAD oscillation diffraction data

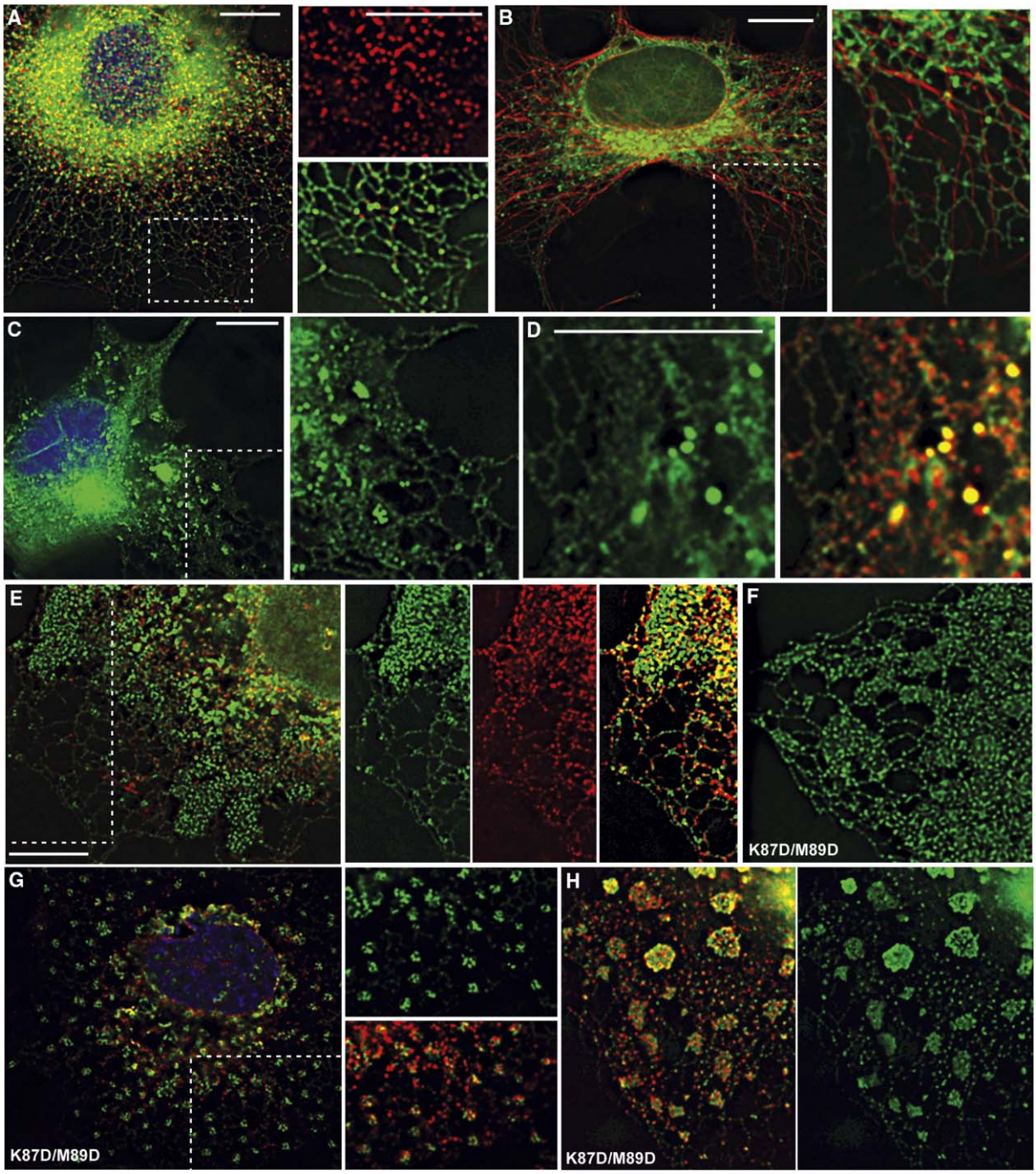

Figure 6. Overexpression of Full-Length VAP or an FFAT Binding Mutant Causes Altered ER Morphology

All scale bars represent 10 μm.

(A) Full-length VAP-GFP (green) expressed in COS7 cells displays a pattern typical for ER proteins. The boxed area is shown in detail in the right-hand panels (top panel, calreticulin; red, bottom panel; VAP-GFP, and calreticulin overlay).

(B) VAP-GFP does not overlay with microtubules. The boxed area is enlarged to show a detailed view of microtubules (red) and VAP-GFP (right panel).

(C) VAP-GFP overexpression often results in areas of intense fluorescence that are continuous with normal-appearing ER (see inset).

(D) Intense fluorescent patches colocalize with calreticulin (red, right panel), indicating that they are likely composed of ER membrane.

(E) A very dense network of ER fills significant areas of the cytoplasm in many cells overexpressing VAP-GFP. The boxed area is shown in detail in the right-hand panels (VAP-GFP, calreticulin, overlay).

(F) These areas of denser ER are more commonly seen in VAP K87D/M89D-GFP-expressing cells.

(G and H) Unlike wild-type VAP, VAP K87D/M89-GFP localizes in some cells to regularly spaced areas of intense fluorescence that are continuous with normal-appearing ER and contain calnexin (red).

were collected at the selenium peak wavelength to d_{min} = 2.8 Å resolution using inverse beam geometry in 5° wedges, and a native diffraction data set to d_{min} = 1.9 Å resolution was also collected (Table 2). Diffraction data were processed with Mosflm/Scala (CCP4, 1994).

Structure Determination and Refinement

For VAP-A (1–125), the six expected selenium sites were found in anomalous difference Patterson maps calculated using the peak wavelength with an automated Patterson heavy atom search method (Grosse-Kunstleve and Brunger, 1999). MAD phasing and density modification were carried out in CNS (Brunger et al., 1998) and resulted in a readily interpretable experimental electron density map. A partial model was built automatically with wARP (Perrakis et al., 1999), and the remainder of the model was built with the program O (Jones et al., 1991). Model refinement was monitored using the free R value (Brunger, 1992) computed from a randomly omitted 10% of the observed diffraction data. Refinement was carried out in CNS using alternating rounds of simulated annealing, torsion angle molecular dynamics (Rice and Brunger, 1994), restrained B factor refinement (Hendrickson, 1985), and model rebuilding. The final model contains one N-terminal expression-construct-derived residue, followed by residues 1–125 of VAP. The final model has excellent stereochemistry (no residues in the disallowed region of the Ramachandran plot), and R and R_{free} values of 22.1% and 24.2%, respectively.

The VAP-FFAT complex crystallized in space group P1. Although data could be processed in space group P3(2)21, a 1 Å translation along Z for molecules obeying the symmetry operators [x – y, –y, –z + 1/3], [–x, –x + y, –z – 1/3], or [y, x, –z] caused refinement to converge poorly. Electron density for the bound FFAT peptide was clear, and refinement proceeded normally in space group P1. The 36 selenium sites from the 6 VAP molecules in the P1 cell were found by molecular replacement using the VAP-A (1–125) model in CNS. SAD phasing and density modification were carried out in CNS using a molecular envelope generated with the VAP-A (1–125) coordinates with MAMA (Kleywegt and Jones, 1999). Density-modified SAD phases were of reasonable quality. After minor rebuilding of the VAP-A (1–125) model and addition of residues from the FFAT peptide, refinement was carried out in CNS with SAD experimental phases as outlined above. The bulk anisotropic B factor was somewhat high, and addition of individual restrained B factors showed no improvement over group-restrained B factor refinement. Translation, libration, and screw rotation (TLS) refinement (Winn et al., 2001) in REFMAC with six TLS groups, each consisting of a VAP-A (1–125) domain with bound peptide, improved both R_{free} and R values by 3%–4%. Tight NCS restraints were used for all atoms throughout refinement. The final model contains ORP1 residues 473–481 and VAP residues 4–125, except for VAP residues 98 and 99, which had uninterpretable electron density. ORP1 residue 472 was not observed, and side chain density was not observed for ORP1 residues 473–475 (occupancies were set to zero for these residues). The final model has no residues in the disallowed region of the Ramachandran plot and R and R_{free} values of 22% and 26%, respectively. Molecular graphics were generated with Pymol (DeLano, 2002).

Gel Shift Assay

Native gel electrophoresis was carried out using 8%–25% native Phast (Pharmacia) gels with native buffer strips (0.88 M L-alanine, 0.25 M Tris [pH 8.8], and 1 mM EDTA). Samples were mixed and incubated for at least 30 min in 50 mM HEPES (pH 7.5), 150 mM NaCl, 5 mM DTT before loading the gel.

Yeast Growth Assay

SCS2 was amplified from genomic DNA with upstream primer 5′-GTCAGAGCACTGAACGAGG-3′ and downstream primer 5′-CGC CTACTACACTAGGGAAACC-3′. The PCR product contained the SCS2 cDNA sequence (CDS), plus 506 bp upstream and 287 bp downstream of the SCS2 gene. The PCR product was first inserted into the pCR-Blunt II-TOPO vector (Invitrogen) and then subcloned as an EcoRI fragment into pRS313 (Sikorski and Hieter, 1989) and sequenced. Yeast growth assays were performed by making a suspension of $\sim 2 \times 10^{-7}$ cells per ml, and a series of 10-fold dilutions were spotted onto SDC –inositol –histidine medium and incubated at 37°C for 2 days.

Fluorescence Microscopy and Image Processing

For experiments in COS7 cells, full-length rat VAP-A (residues 1–242) was subcloned as an XhoI-HindIII fragment in pEGFP-N1 (Clontech) and confirmed by sequencing. COS7 cells were grown in DMEM with 10% serum. Cells were transfected with Lipofectamine 2000 (Invitrogen) and plated on collagen-coated glass coverslips. Cells were fixed 48 hr after transfection in 4% paraformaldehyde or 0.3% glutaraldehyde for costaining of microtubules. For tubulin staining, DM1α (Sigma) was used at 1/500. Polyclonal antibodies to calnexin and calrecticulin were diluted 1/1000 (Stressgen). Cells were mounted in Vectashield mounting medium or Vectashield with DAPI (Vector Laboratories, Burlingame, CA). Image z stacks were collected in 0.20 μm steps on an Olympus IX-70 inverted microscope with a 60X 1.4 N.A. oil-immersion objective (Olympus) and were captured by a cooled CCD camera (Photometrics). Images were collected and processed with Delta Vision deconvolution software (Applied Precision, Seattle, WA) on a Silicon Graphics workstation (Silicon Graphics).

Supplemental Data

Supplemental Data including Figure S1, which contains alignments of VAP and FFAT proteins, and Figure S2, which contains SEC-MALLS analysis of VAP-FFAT complex solution behavior, are available at http://www.structure.org/cgi/content/full/13/7/1035/DC1/.

Acknowledgments

We thank L. Rice for advice on SAD data collection; R. Grosse-Kunstleve, N. Sauter, and P. Adams for advice while solving the structures; Corie Ralston for assistance with data collection; and D. Starcevic, M. Bowen, M. Breidenbach, J. Hyman, S. Fukai, R. Reimer, D. Hattendorf, K. Slep, S. Jaswal, J. Kohler, J. Christianson, R. Kopito, and J. Nelson for discussions and critical reading of the manuscript. Diffraction data were collected at the Lawrence Berkeley National Laboratory Advanced Light Source beamline 8.2.1 and at the Stanford Synchrotron Radiation Laboratory (SSRL), a national user facility operated by Stanford University on behalf of the U.S. Department of Energy (Office of Basic Energy Sciences). The SSRL Structural Molecular Biology Program is supported by the Department of Energy (Office of Biological and Environmental Research) and by the National Institutes of Health (National Center for Research Resources, Biomedical Technology Program).

Received: March 7, 2005
Revised: April 4, 2005
Accepted: April 4, 2005
Published: July 12, 2005

References

Amarilio, R., Ramachandran, S., Sabanay, H., and Lev, S. (2005). Differential regulation of ER structure through VAP-Nir protein interaction. J. Biol. Chem. *280*, 5934–5944.

Baumann, O., and Walz, B. (2001). Endoplasmic reticulum of animal cells and its organization into structural and functional domains. Int. Rev. Cytol. *205*, 149–214.

Bernard, A., and Payton, M. (1995). Fermentation and growth of *Escherichia coli* for optimal protein production. Current Protocols in Protein Science *5*, 1–18.

Brickner, J.H., and Walter, P. (2004). Gene recruitment of the activated *INO1* locus to the nuclear membrane. PLoS Biol. *2*, E342.

Brunger, A. (1992). The free R value: a novel statistical quantity for assessing the accuracy of crystal structures. Nature *355*, 472–474.

Brunger, A.T., Adams, P.D., Clore, G.M., DeLano, W.L., Gros, P., Grosse-Kunstleve, R.W., Jiang, J.S., Kuszewski, J., Nilges, M., Pannu, N.S., et al. (1998). Crystallography & NMR system: a new

software suite for macromolecular structure determination. Acta Crystallogr. D Biol. Crystallogr. *54*, 905–921.

Bullock, T.L., Roberts, T.M., and Stewart, M. (1996). 2.5 Å resolution crystal structure of the motile major sperm protein (MSP) of *Ascaris suum*. J. Mol. Biol. *263*, 284–296.

CCP4 (Collaborative Computational Project, Number 4) (1994). The CCP4 suite: programs for protein crystallography. Acta Crystallogr. D Biol. Crystallogr. *50*, 760–763.

DeLano, W.L. (2002). The PyMOL Molecular Graphics System (http://www.pymol.org).

Foster, L.J., Weir, M.L., Lim, D.Y., Liu, Z., Trimble, W.S., and Klip, A. (2000). A functional role for VAP-33 in insulin-stimulated GLUT4 traffic. Traffic *1*, 512–521.

Grosse-Kunstleve, R.W., and Brunger, A.T. (1999). A highly automated heavy-atom search procedure for macromolecular structures. Acta Crystallogr. D Biol. Crystallogr. *55*, 1568–1577.

Haaf, A., Butler, P.J., Kent, H.M., Fearnley, I.M., Roberts, T.M., Neuhaus, D., and Stewart, M. (1996). The motile major sperm protein (MSP) from *Ascaris suum* is a symmetric dimer in solution. J. Mol. Biol. *260*, 251–260.

Hendrickson, W.A. (1985). Stereochemically restrained refinement of macromolecular structures. Methods Enzymol. *115*, 252–270.

Hendrickson, W.A. (1991). Determination of macromolecular structures from anomalous diffraction of synchrotron radiation. Science *254*, 51–58.

Jones, T.A., Zou, J.Y., and Cowan, S.W. (1991). Improved methods for building protein models in electron density maps and the location of errors in these models. Acta Crystallogr. A *47 (Pt 2)*, 110–119.

Kagiwada, S., Hosaka, K., Murata, M., Nikawa, J., and Takatsuki, A. (1998). The *Saccharomyces cerevisiae* SCS2 gene product, a homolog of a synaptobrevin-associated protein, is an integral membrane protein of the endoplasmic reticulum and is required for inositol metabolism. J. Bacteriol. *180*, 1700–1708.

Kleywegt, G.J., and Jones, T.A. (1999). Software for handling macromolecular envelopes. Acta Crystallogr. D Biol. Crystallogr. *55*, 941–944.

Loewen, C.J., and Levine, T.P. (2005). A highly conserved binding site in VAP for the FFAT motif of lipid binding proteins. J. Biol. Chem. *280*, 14097–14104.

Loewen, C.J., Roy, A., and Levine, T.P. (2003). A conserved ER targeting motif in three families of lipid binding proteins and in Opi1p binds VAP. EMBO J. *22*, 2025–2035.

Pennetta, G., Hiesinger, P., Fabian-Fine, R., Meinertzhagen, I., and Bellen, H. (2002). *Drosophila* VAP-33A directs bouton formation at neuromuscular junctions in a dosage-dependent manner. Neuron *35*, 291–306.

Perrakis, A., Morris, R., and Lamzin, V.S. (1999). Automated protein model building combined with iterative structure refinement. Nat. Struct. Biol. *6*, 458–463.

Rice, L.M., and Brunger, A.T. (1994). Torsion angle dynamics: reduced variable conformational sampling enhances crystallographic structure refinement. Proteins *19*, 277–290.

Roberts, T.M., and Stewart, M. (2000). Acting like actin. The dynamics of the nematode major sperm protein (msp) cytoskeleton indicate a push-pull mechanism for amoeboid cell motility. J. Cell Biol. *149*, 7–12.

Rost, B., and Liu, J. (2003). The PredictProtein server. Nucleic Acids Res. *31*, 3300–3304.

Russ, W.P., and Engelman, D.M. (2000). The GxxxG motif: a framework for transmembrane helix-helix association. J. Mol. Biol. *296*, 911–919.

Sikorski, R.S., and Hieter, P. (1989). A system of shuttle vectors and yeast host strains designed for efficient manipulation of DNA in *Saccharomyces cerevisiae*. Genetics *122*, 19–27.

Skehel, P.A., Martin, K.C., Kandel, E.R., and Bartsch, D. (1995). A VAMP-binding protein from Aplysia required for neurotransmitter release. Science *269*, 1580–1583.

Skehel, P.A., Fabian-Fine, R., and Kandel, E.R. (2000). Mouse VAP33 is associated with the endoplasmic reticulum and microtubules. Proc. Natl. Acad. Sci. USA *97*, 1101–1106.

Soussan, L., Burakov, D., Daniels, M.P., Toister-Achituv, M., Porat, A., Yarden, Y., and Elazar, Z. (1999). ERG30, a VAP-33-related protein, functions in protein transport mediated by COPI vesicles. J. Cell Biol. *146*, 301–311.

Van Duyne, G.D., Standaert, R.F., Karplus, P.A., Schreiber, S.L., and Clardy, J. (1993). Atomic structures of the human immunophilin FKBP-12 complexes with FK506 and rapamycin. J. Mol. Biol. *229*, 105–124.

Weir, M.L., Xie, H., Klip, A., and Trimble, W.S. (2001). VAP-A binds promiscuously to both v- and tSNAREs. Biochem. Biophys. Res. Commun. *286*, 616–621.

Winn, M.D., Isupov, M.N., and Murshudov, G.N. (2001). Use of TLS parameters to model anisotropic displacements in macromolecular refinement. Acta Crystallogr. D Biol. Crystallogr. *57*, 122–133.

Wyles, J.P., and Ridgway, N.D. (2004). VAMP-associated protein-A regulates partitioning of oxysterol-binding protein-related protein-9 between the endoplasmic reticulum and Golgi apparatus. Exp. Cell Res. *297*, 533–547.

Wyles, J.P., McMaster, C.R., and Ridgway, N.D. (2002). Vesicle-associated membrane protein-associated protein-A (VAP-A) interacts with the oxysterol-binding protein to modify export from the endoplasmic reticulum. J. Biol. Chem. *277*, 29908–29918.

Accession Numbers

The VAP-A (1–125) and VAP-A (1–125) + FFAT complexes were deposited in the Protein Data Bank under codes 1Z9L and 1Z9O, respectively.